2013-01-0582

Intra-Pipe Restriction Non-Homentropic Boundary Resolution Method

Felipe Castillo
Renault SAS, GIPSA Lab

Emmanuel Witrant, Luc Dugard
UJF Grenoble 1/CNRS/GIPSA Lab

Vincent Talon
Renault SAS

David Chalet, Pascal Chesse
LUNAM Université, Ecole Centrale de Nantes

ABSTRACT

A complete non-homentropic boundary resolution method for a flow upstream and downstream an intra-pipe restriction is considered in this article. The method is capable of introducing more predictable quasi-steady restriction models into the boundary problem resolution without adding artificial discharge coefficients. The traditional hypothesis of isentropic contraction, typically considered for the boundary resolution, is replaced by an entropy corrected method of characteristics (MOC) in order to be consistent with a non-homentropic formulation. The boundary resolution method is designed independently of the quasi-steady restriction models which allows obtaining a greater modeling flexibility when compared with traditional methods. An experimental validation at unsteady conditions is presented using different restriction quasi-steady models to illustrate the effectiveness of the proposed boundary resolution method in terms of predictability as well as flexibility.

INTRODUCTION

In the recent years, Diesel engine emissions regulations have become stricter and achieving simultaneously the emissions legislations and the demanded engine drivability has become a very challenging issue. Although significant improvements have been made over the past years, there are still many challenges to address in order to meet the future emissions regulations. The introduction of sophisticated alternative combustion modes such as homogeneous charge compression ignition (HCCI), low temperature combustion (LTC) and premixed controlled compression ignition (PCCI) offer a great potential to reduce the engine emissions levels [1] [2] [15]. However, these new modes require different fueling strategies and in-cylinder conditions, thus creating the need for more complex, reliable and precise control systems and technologies.

Dual-loop exhaust gas recirculation (EGR) with both high and low-pressure recirculations, is one of the new strategies proposed to achieve the appropriate conditions to implement multiple combustion modes [13]. However, ensuring the adequate in-cylinder conditions is still a very difficult task, as the introduction of the EGR brings many control challenges due to the lack of EGR flow rates and mass fraction measurements. An efficient control of the in-cylinder combustion and engine-out emissions not only involves the total in-cylinder EGR amount, but also the ratio between the high-pressure EGR (HP-EGR) and the low-pressure EGR (LP-EGR). Indeed, this ratio is crucial as the gas temperature and composition are significantly affected. The HP-EGR gas is used during the beginning of a cycle in order to obtain combustions with elevated temperatures and therefore heating up as fast as possible the exhaust post-treatment systems. As LP-EGR is cooler, it has a higher density and therefore, it allows introducing more mass and more EGR into the cylinders. The LP-EGR reduces the engine-out NOx emission without excessive smoke as it is filtered by the particle filter. Controlling the air fractions in the intake manifold is an efficient approach to control the in-cylinder EGR amount [3] [10]. For engines with dual EGR systems, the air fraction upstream of the compressor indicates the LP-EGR rate and the air

fraction in the intake manifold indicates the total EGR rate. Therefore, if the air fractions in each section are controlled, then the HP and LP-EGR can also be controlled efficiently.

Controlling the air mass fraction is a difficult task, because direct measurement of the air fraction is not available on the production engines and the dynamics of the admission air-path can be highly complex. One of the actual problems to control the air mass fraction in the intake manifold is the EGR mass transport time. This phenomenon is much more significant in the LP-EGR as the distance that the gas travels in the engine air-path is much longer than the one associated with HP-EGR. Indeed, this phenomenon causes a degradation of the overall engine emission performance during the strong transients. Several air mass fraction/EGR rate estimation methods have been proposed in the literature to overcome some of the actual limitations [10] [17] [14]. However, most of these estimation techniques are based on 0-D engine modeling, which does not permit to take into account the mass transport time.

One dimensional modeling (1-D) allows estimating the mass transport time in the air path of the engine, but at the price of dealing with more complex problems such as boundary conditions resolution. One of the boundary conditions to take into account is the intra-pipe restriction boundary, which is the focus of this study. The classical restriction boundary problem resolution methods are generally based on an isentropic flow assumption, which simplifies the boundary problem significantly. However, this hypothesis in not verified experimentally as higher flow rates are systematically obtained through the restriction. Therefore, experimental discharge coefficients are generally introduced to deal with this issue artificially [8] [9] [16]. Nevertheless, the drawback of this strategy is that experimental measurements must be performed, which increases the costs of the model calibration. Additionally, in the case where no experimental data are available to determine the discharge coefficients, simulation results can be in total disagreement with bench measurements. An other technique consists on using a computational fluid dynamics code as a numerical test bench [7] [16]. However, this technique is time consuming and experimental results are necessary in order to validate the numerical bench. This motivates the search for restriction models and intra-pipe restriction boundary resolution methods capable of offering a greater predictability and more flexibility in terms of modeling capabilities.

In [12], this issue has been considered for the non-homentropic inflow boundary problem and in [6], the same has been done for the outflow boundary. In this paper, an innovative, non-hometropic consistent, intra-pipe restriction boundary resolution method independent of the quasi-steady restriction models is developed with the purpose of increasing the predictability and the flexibility of the 1-D modeling platforms for control purposes. In other words, this proposal allows the introduction of more predictable quasi-steady restriction models into the boundary problem resolution without the need of adding artificial discharge coefficients. A 1-D aerodynamics modeling platform is developed in order to provide an accurate white box model to perform control and estimation on the mass transport phenomenon. For example, fresh mass fraction estimators that take into account the mass transport time. The study detailed in this paper has a practical application on EGR and admission throttle flow modeling, among many others. To solve the restriction boundary condition, a specific resolution of Euler's equations needs to be implemented. In this work, a method of characteristics, modified to take into account the non-homentropic flows across a restriction is considered due to its satisfactory robustness and accuracy.

The paper is organized as follows. First, the equations and hypothesis introduced to build quasi-steady restriction models are described. Then, a modified method of characteristics (MOC) is proposed to develop an innovative non-homentropic restriction boundary resolution methodology. This allows implementing different restriction models without modifying the boundary resolution scheme, while always being physically consistent with a non-homentropic formulation. Additionally, a Newton-Raphson algorithm is introduced in the scheme, along with an extrapolation to initialize the resolution method. It increases the efficiency of the numerical method in terms of required iterations as well as the accuracy of the solution. The predictability, flexibility and the unsteady performance of the proposed boundary resolution method are compared and validated using experimental measurements as a reference.

QUASI-STEADY INTRA-PIPE RESTRICTION MODELS

In this section, some of the equations and assumptions on quasi-steady restriction models given in the literature are presented as well as how put these models into data-maps. Let us introduce an illustrative schematic of the restriction to present the boundary problem.

As depicted in Figure 1, the plane 3 is located upstream the restriction, just before the gas contraction, the plane 2 is located at the restriction throat and the plane 1 is found downstream the restriction after the

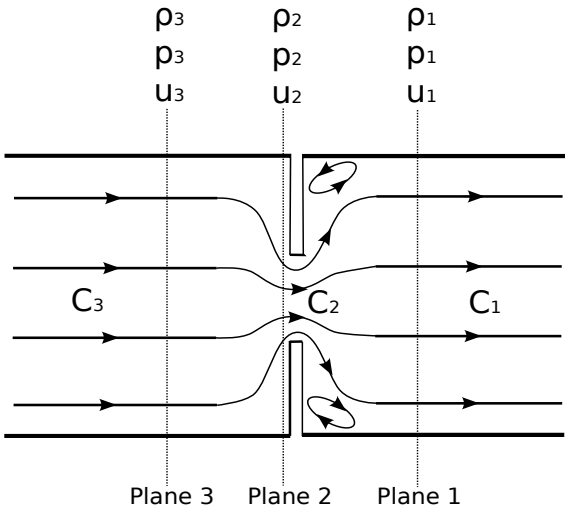

Figure 1: Intra-pipe Restriction Schematic

gas expansion. The gas comes from a pipe of cross-sectional area C_3 and passes through the restriction throat as a jet of cross-sectional area C_2. Then, the gas expands in a pipe of cross-sectional area C_1. At the time when quasi-steady models were developed, desktop computers memory did not allow the solutions to be pre-calculated into data-maps. Indeed, Newton-Raphson algorithms were used to solve the boundary problem, introducing an iterative problem at each time step. The main issue of this approach is that the convergence algorithm had to be modified for each specific model. Pre-processed data-maps at the interface between the quasi-steady model and the 1-D in pipe numerical scheme are thus advantageous. Therefore, all the models developed in this section are put into data-maps. These data-maps are then used in the proposed boundary resolution method presented in the following sections.

As proposed in [11], the restriction boundary problem can be considered as an outflow boundary problem together with an inflow boundary problem. Most of the approaches assume to have an isentropic contraction between planes 3 and 2 and a momentum conservation between planes 2 and 1 (e.g see Benson's proposal [4]). However, there have been other propositions such as in [6], where a momentum formulation has been used to model the outflow boundary (planes 3 and 2), which has shown to exhibit a better performance in terms of predictability than the traditional isentropic contraction approach. In [12], different inflow quasi-steady models have been considered and it has been shown that a pressure constant inflow model presents better predictability than a momentum-based one. This motivates the search for a non-homentropic formulation for the restriction boundary resolution, capable of using alternative modeling strategies.

Consider the following hypotheses in order to formulate the intra-pipe restriction models:

H-1: the states are quasi-steady over the three planes;

H-2: the energy is conserved in all three planes;

H-3: the conservation of mass applies at all planes;

H-4: no change of the gas heat ratio with respect to the temperature and EGR percentage is considered for the data-map generation.

The hypothesis H-4 is reasonable for an engine air-path operating with EGR because the effect of the heat ratio variation on the data-maps is much smaller than the effect of the quasi-steady model formulation as detailed in Appendix I. Thus, the variation of the heat ratio is not critical for control and estimation purposes. Nevertheless, if the impact of this variation is required, it can be considered by adding a supplementary input to the quasi-steady model data-map.

According to Figure 1, the conservation of energy can be written as [18]:

$$a_{tot}^2 = a_1^2 + \frac{\gamma-1}{2}u_1^2 = a_2^2 + \frac{\gamma-1}{2}u_2^2 = a_3^2 + \frac{\gamma-1}{2}u_3^2 \tag{1}$$

where a is the speed of the sound, u is the particle speed and γ is the specific heat ratio. The total speed of the sound is defined as:

$$a_{tot} = \sqrt{a^2 + \frac{\gamma-1}{2}u^2} \tag{2}$$

The mass conservation can be expressed as:

$$\frac{C_1 p_1 u_1}{a_1^2} = \frac{C_2 p_2 u_2}{a_2^2} = \frac{C_3 p_3 u_3}{a_3^2} \tag{3}$$

Let us review some of the outflow and inflow models considered in this work.

INFLOW MODELS

The procedure to obtain the inflow quasi-steady models is not detailed in this work, only the main results of

a pressure constant and a momentum-based inflow models are presented. For more details on these models, see [11] and [12]. Equations (4) and (5) present the model obtained using the constant pressure model:

$$U_1^2 + \left(\frac{2A_2^2}{\Phi_1(\gamma-1)U_2}\right)U_1 - \frac{2}{\gamma-1} = 0 \tag{4}$$

$$\frac{p_1}{p_2} = 1 \tag{5}$$

where $\Phi_1 = C_2/C_1$, $U = u/a_{tot}$ is the non-dimensional particle speed and $A = a/a_{tot}$ is the non-dimensional speed of the sound. From equation (1), the non-dimensional speed of the sound can be defined in terms of the non-dimensional particle speed as $A = \sqrt{1 - \frac{\gamma-1}{2}U^2}$. The momentum-based inflow model is described as follows:

$$U_1^2 + \left(\frac{2}{\gamma+1}\right)\left(\frac{A_2^2}{\Phi_1 U_2} + \gamma U_2\right)U_1 + \frac{2}{\gamma+1} = 0 \tag{6}$$

$$\frac{p_1}{p_2} = \frac{1 + \gamma\Phi_1\left(\frac{U_2}{A_2}\right)^2}{1 + \gamma\left(\frac{U_1}{A_1}\right)^2} \tag{7}$$

These models allow establishing a quadratic relationship between the throat and the downstream non-dimensional particle speed. Also, an expression for the pressure ratio p_1/p_2 is obtained. In [12], it has been shown that the constant pressure inflow model (4) presents a better predictability than the momentum-based model (6).

OUTFLOW MODELS

Similar to the inflow case, only the main results of two outflow models are considered: an isentropic contraction and a momentum-based models. For further details on the models see [6]. The following presents the outflow isentropic model:

$$U_3 = \Phi_3 U_2\left[\left(\frac{1}{A_2}\right)^2 - \frac{\gamma-1}{2}\left(\frac{U_3}{A_2}\right)^2\right]^{\frac{-1}{\gamma-1}} \tag{8}$$

$$\frac{p_3}{p_2} = \left(\frac{a_3}{a_2}\right)^{\frac{2\gamma}{\gamma-1}} \tag{9}$$

where $\Phi_3 = C_2/C_3$. The momentum-based approach is given as follows:

$$\left(\gamma - \Phi_3\frac{\gamma-1}{2}\right)U_3^2 + \left(\frac{A_2^2}{U_2} + \gamma U_2\right)U_3 + \Phi_3 = 0 \tag{10}$$

$$\frac{p_3}{p_2} = \frac{1 + \gamma\left(\frac{U_2}{A_2}\right)^2}{1 + \frac{\gamma}{\Phi_3}\left(\frac{U_3}{A_3}\right)^2} \tag{11}$$

In [6], it has been shown that the momentum-based model has a better predictability than the isentropic based one. To obtain the models under sonic flow at the throat, meaning that $U_2 = A_2$, the non-dimensional speeds U_2 and A_2 are replaced in (4) - (11) by $U_2 = A_2 = \sqrt{\frac{2}{\gamma+1}}$ (energy conservation (1)).

RESTRICTION MODELS AND DATA-MAP GENERATION

As previously mentioned, the restriction model can be considered as a combination of an inflow and an outflow models. Therefore, four different quasi-steady restriction models can be obtained from models given by (4), (6), (8) and (10). To illustrate an example of how the restriction model is formulated, both momentum-based approaches ((6) and (10)) are considered. The link between the models is done by the non-dimensional speeds U_2 and A_2 as well as with the pressure p_2. These quantities are shared by both quasi-steady models. Taking this into account, the following restriction model is obtained:

$$\begin{aligned}\left(\gamma - \Phi_3\frac{\gamma-1}{2}\right)U_3^2 + \left(\frac{A_2^2}{U_2} + \gamma U_2\right)U_3 + \Phi_3 = 0\\ U_1^2 + \left(\frac{2}{\gamma+1}\right)\left(\frac{A_2^2}{\Phi_1 U_2} + \gamma U_2\right)U_1 + \frac{2}{\gamma+1} = 0\end{aligned} \tag{12}$$

$$\frac{p_1}{p_3} = \frac{1 + \gamma\Phi_1\left(\frac{U_2}{A_2}\right)^2}{1 + \gamma\left(\frac{U_1}{A_1}\right)^2}\frac{1 + \frac{\gamma}{\Phi_3}\left(\frac{U_3}{A_3}\right)^2}{1 + \gamma\left(\frac{U_2}{A_2}\right)^2} \tag{13}$$

This model gives for every U_2, a respective U_1, U_3 and p_1/p_3. With the purpose of avoiding the solution of (12) every time step, a data-map is generated to store the solution which then can be easily re-calculated by using look-up table techniques along with a trilinear interpolation. These data-maps can be configured to solve p_1/p_3 and U_1 as follows:

$$\frac{p_1}{p_3} = Datamap_p(U_3, \Phi_1, \Phi_3) \tag{14}$$

and

$$U_1 = Datamap_U(U_3, \Phi_1, \Phi_3) \tag{15}$$

where U_3, Φ_1 and Φ_3 are the data-map's inputs. In order to obtain these data-maps, the following procedure is proposed:

1. set a range of U_2 equal to $\left[0, \sqrt{\frac{2}{\gamma+1}}\right]$ (Subsonic range), A_2 is found using (1);
2. with U_2 and A_2, (12) is solved numerically (or analytically depending on the model) to get U_1 and U_3. To find A_1 and A_3 use the energy conservation equation once again;
3. using U_1 and U_3 and the pressure ratio equation (for example (13)), the values of p_1/p_3 can be found;
4. to include the sonic solution in the data-map, solve the model equations with $U_2 = A_2 = \sqrt{\frac{2}{\gamma+1}}$

Figure 2 presents two data-maps obtained using both momentum-based models and the outflow isentropic model along with the constant pressure inflow model.

As depicted in Figure 2, there are important differences between both approaches. The isentropic constant-pressure model presents greater particle speeds than the momentum-based strategy. Later in the validation section, it is shown how this affects the predictability of the restriction modeling. Restrictions with different geometries, such as control valves for example, can create different data-maps from the ones obtained with simple orifices. However, as previously mentioned, the boundary resolution method presented in the next section is independent of the quasi-steady models, implying that any control valve model can be used without modifying the boundary resolution method. In this work, for sake of simplicity, the simple orifices are

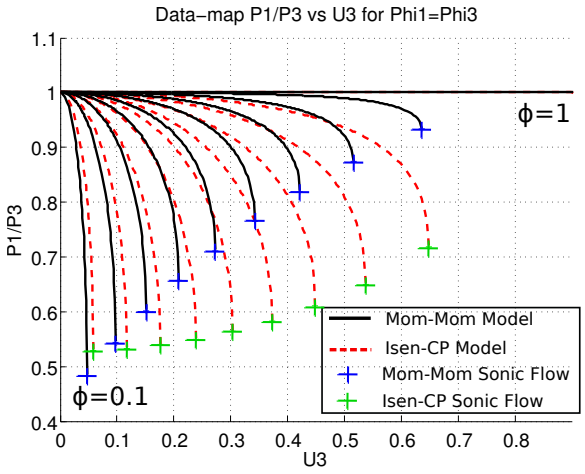

Figure 2: Intra-pipe restriction data-maps comparison (see page 7 for details on the notation)

used to illustrate the benefits of using the proposed non-homentropic formulation for the boundary resolution. Using a model independent boundary resolution method will allow creating control laws independently of the restriction model which is of great interest for control applications.

INTRA-PIPE RESTRICTION BOUNDARY PROBLEM RESOLUTION

With the restriction quasi-steady model available in data-maps, now it is required to create an interaction between these data-maps and the in-pipe resolution scheme (MacCormack + Total Variation Diminishing (TVD) has been considered in this work). This interaction is commonly known as the boundary resolution method. A modified method of characteristics (MOC), that takes into account the change of entropy level, has proved to be a versatile method to create this interaction [6] [18] [12]. However, in most approaches seen in the literature, an isentropic contraction is systematically considered to solve the boundary problem. The main contribution of this work is to formulate a restriction boundary resolution method that does not take into account the isentropic contraction assumption. Moreover, a method capable of integrating any quasi-steady model in the form of (14) and (15) is considered. Additionally, some other improvements are brought to the method such as a more efficient numerical method and speed of the sound and pressure reference free formulation.

PROPOSED METHOD

Figure 3 shows the schematic of the MOC approach used in this study to solve the boundary problem. The index D represents the value of a variable upstream the boundary, the index F represents the value of a variable at the downstream boundary, the index L

represents the interpolated point between D and $D-1$ where the trajectory $u+a$ crosses at time n and the index R represents the interpolated point between F and $F+1$ where the trajectory $a-u$ crosses at time n. The index S is associated to the trajectory u at time n.

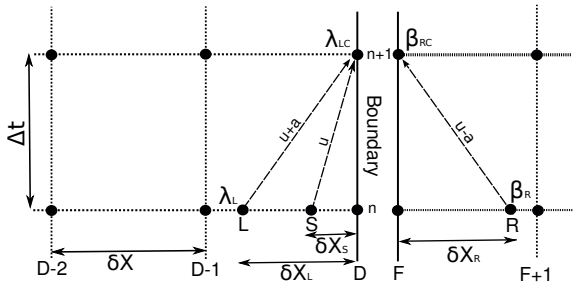

Figure 3: Characteristics Restriction Boundary

Along the trajectories $u+a$, $u-a$ and u, the following conditions are satisfied (called Riemann invariants) for homentropic flow [18]:

$$\lambda = a_D^{n+1} + \frac{\gamma-1}{2}u_D^{n+1} = a_L^n + \frac{\gamma-1}{2}u_L^n \qquad (16)$$

$$\beta = a_F^{n+1} - \frac{\gamma-1}{2}u_F^{n+1} = a_R^n - \frac{\gamma-1}{2}u_R^n \qquad (17)$$

$$s_D^{n+1} = s_S^n \qquad (18)$$

where s_S is the entropy at the point S of Figure 3. Equation (18) implies that:

$$\frac{p_D^{n+1}}{\left(\rho_D^{n+1}\right)^\gamma} = \frac{p_S^n}{\left(\rho_S^n\right)^\gamma} \qquad (19)$$

However, in many cases the homentropic assumption is not satisfied and the MOC has to be modified to take into account the difference of entropy across the restriction. The changes of entropy due to heat transfer and friction at the boundaries are neglected as the change over one finite element is small in comparison with the change along the whole tube. In [6], a modification of (16) is developed with the purpose of taking into account the change of entropy level at the boundary, removing the need for defining the traditionally used pressure and speed of the sound references. This allows the entropy correction to be written directly in terms of the available quantities at time n. The same can also be done with (17), which gives:

$$u_D^{n+1} = \frac{2}{\gamma-1}\left(\lambda_L^n - a_L^n\left(\frac{p_D^{n+1}}{p_L^n}\right)^{\frac{\gamma-1}{2\gamma}}\right) \qquad (20)$$

$$u_F^{n+1} = \frac{2}{\gamma-1}\left(\beta_R^n - a_R^n\left(\frac{p_F^{n+1}}{p_R^n}\right)^{\frac{\gamma-1}{2\gamma}}\right) \qquad (21)$$

For the solution of the boundary problem, six unknowns have to be solved (u_D^{n+1}, a_D^{n+1}, p_D^{n+1}, u_F^{n+1}, a_F^{n+1} and p_F^{n+1}). Therefore, six equations have to be available. In this work, the replacement of the traditionally isentropic contraction equation by a modification of the Riemann invariant (18) is proposed in order to be consistent with the non-homentropic formulation. The procedure to modify (18) is well detailed in [6]. The following equation is obtained:

$$a_D = \sqrt{\gamma s_S^{\frac{1}{\gamma}} p_D^{\frac{\gamma-1}{2\gamma}}} \qquad (22)$$

Note that (22) relates directly the speed of the sound with the pressure upstream the restriction. The energy and the mass conservation, (15) (20), (21) and (22) correspond to the six equations required for the boundary resolution. The solution of this system, however, is not analytically possible to find. Thus, a numerical procedure is required to solve the boundary problem. Different numerical methods could be used to achieve this, such as the ones proposed in [4] and in [6]. The numerical procedure presented in [6], which is a Newton-Raphson-based algorithm implemented with finite differences along with an initialization using an extrapolation, is considered in this work as it has shown good results in terms of accuracy as well as number of iterations. Consider the following initialization for the numerical method:

$$p_D^{it} = 2p_{D-1} - p_{D-2} \qquad (23)$$

where p_D^{it} is the initial pressure for the iterative algorithm at the boundary. Equation (23) is a linear extrapolation of the pressure at the boundary using the two closest finite elements in the tube. This extrapolation can be very close to the solution, specially during the

steady-state conditions, avoiding the use of the iterative algorithm, which decreases the calculation time. With p_D^{it} available, is it possible to calculate with (20) and (22), u_D^{it} and a_D^{it} respectively. The total speed of the sound a_{tot}^{it} is calculated with (2) to find U_D^{it}.

With (14), the downstream pressure is found. Then it is used to calculate U_F^{it} with (21). However, in order to check the consistency of the solution, in other words to see whether p_D^{it} is a solution, the following function is defined:

$$f = \mid U_F^{it} - datamap_U(U_D^{it}, \Phi_1, \Phi_3) \mid < \epsilon \qquad (24)$$

where $\epsilon > 0$ sets the convergence accuracy. However, nothing guaranties that (23) satisfies the criterion (24). That is why an iterative procedure has to be implemented until (24) is satisfied. Consider the numerical method proposed in [6] to update p_D^{it}:

$$p_D^{it+1} = p_D^{it} - \frac{f\left(p_D^{it}\right)}{\frac{f\left(p_D^{it}+\Delta p\right)-f\left(p_D^{it}\right)}{\Delta p}} \qquad (25)$$

where Δp is a small differential to approximate numerically the derivative $\frac{df}{dp}$. When Δp in (25) is small, a better approximation to the analytic Newton-Raphson algorithm is obtained. (25) will be calculated until the condition (24) is satisfied. The same algorithm has to be considered under sonic flow with the difference that the data-maps are built in this case considering $U_2 = A_2 = \sqrt{\frac{2}{\gamma+1}}$.

Method implementation

To implement the proposed method, consider the following steps:

1. calculate λ_L^n, s_S^n and β_R^n: use (16), (19) and (17), respectively;
2. initialize $p_D^{it} = 2p_{D-1}^{n+1} - p_{D-2}^{n+1}$. This is the linear extrapolation using the two closest nodes inside the pipe where p_{D-1}^{n+1} and p_{D-2}^{n+1} are obtained by the in-pipe numerical scheme,
3. use (22) to calculate a_D^{it} and (20) to compute u_D^{it}
4. calculate the total speed of the sound with (2) and compute the non-dimensional speeds U_D^{it} and A_D^{it};
5. compute $p_D/p_F = datamap_P(U_D^{it}, \Phi_1, \Phi_3)$ using any of the restriction models;
6. calculate U_F^{it} using (21) and the total speed of the sound. Use the energy conservation equation to find A_F^{it};
7. compute (24). If $f < \epsilon$, then return $p_D^{n+1} = p_D^{it}$, $a_D^{n+1} = a_D^{it}$, $u_D^{n+1} = u_D^{it}$, $p_F^{n+1} = p_F^{it}$, $a_F^{n+1} = a_F^{it}$ and $u_F^{n+1} = u_F^{it}$. Otherwise, use (25) to update p_D^{it} and return to the step 3;

EXPERIMENTAL VALIDATION OF THE PROPOSED RESOLUTION METHOD

In this section, an experimental validation of the proposed restriction boundary resolution method is performed. Four different quasi-steady restriction models are considered to illustrate the gain in predictability and flexibility of the proposed non-homentropic formulation. The following models are considered:

- Isentropic outflow and constant pressure inflow model (Isen-CP Model);
- Isentropic outflow and momentum inflow model (Isen-Mom Model);
- Momentum outflow and constant pressure inflow model (Mom-CP Model);
- Momentum outflow and momentum inflow model (Mom-Mom Model);

Figure 5 presents the schematic that describes the experimental setup conceived for the experimental validation of the boundary resolution method. Figure 4 depicts an actual picture of the experimental setup.

The experimental setup consists on a thermally isolated reservoir of volume V_{tank}, a guillotine at the entrance of the tube in order to introduce a shock wave and two pipes connected by a restriction. In order to introduce a change of the entropy level, it is necessary to heat up the gas inside the reservoir. Prior to the guillotine opening, the desired initial gas temperature is set by operating an inlet and an outlet valve connected to the reservoir. These valves are installed in a parallel air heating system not detailed in this work. After the warm-up phase, the valves are closed and remain in this position during the tests. The guillotine position is measured in order to approximate the area ratio of the input restriction during its unsteady conditions.

Three different experiments are presented. Three restriction area ratios are used ($\Phi_1 = \Phi_3 = 0.1$, $\Phi_1 = \Phi_3 = 0.2$ and $\Phi_1 = \Phi_3 = 0.5$) with different

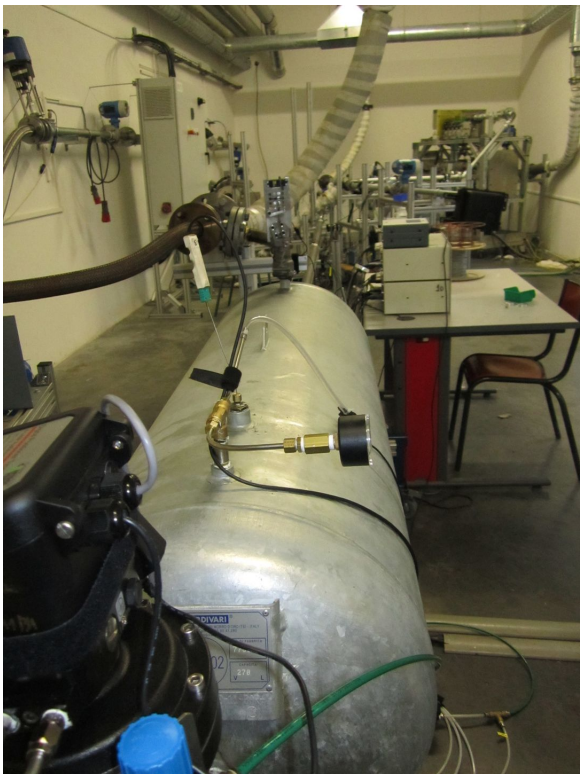

Figure 4: Picture of the experimental setup

initial p_{tank} and T_{tank}. The reservoir pressure and temperature dynamics are modeled using a classical 0-D thermodynamical model which is initialized at $p_{tank}(t = 0)$ and $T_{tank}(t = 0)$. As the reservoir is thermally isolated, no heat wall transfers are considered. The in-pipe numerical scheme is a MacCormack + TVD. The pipes friction and thermal exchanges coefficients have been identified with the setup operating with no restriction. The inflow restriction boundary resolution method presented in [12] with a constant pressure quasi-steady model is considered to model the flow across the guillotine.

Figures 6, 7 and 8 show the results obtained for three different experimental conditions. In Figure 6, $\Phi_1 = \Phi_3 = 0.1$ and $p_{tank}(t = 0) \approx 1.4 \times 10^5$ [Pa]. In Figure 7, $\Phi_1 = \Phi_3 = 0.2$ and $p_{tank}(t = 0) \approx 1.2 \times 10^5$ [Pa] and in Figure 8, $\Phi_1 = \Phi_3 = 0.5$ and $p_{tank}(t = 0) \approx 1.1 \times 10^5$ [Pa]. The initial reservoir temperature for all the experiments is $T_{tank}(t = 0) \approx 500K$.

The pressure decrease of the reservoir depends directly on the mass flow rate through the guillotine, which is a good indicator for identifying the accuracy of each modeling approach (see pressure @ 202mm of Figures 6, 7 and 8). It is important to take into account that the time responses of the sensors have to be taken into account for the results analysis, for all the temperature measurements. The instantaneous pressures are measured with Kistler 4049A10SP22 piezoresistive sensors. The temperatures are measured with thermosensors of type K with a diameter of 0.075 mm.

Model/Variable	Model	p_1	p_2
$\Phi_1 = \Phi_3 = 0.1$	Isen-CP	13.1 %	20.2 %
	Mom-CP	5.6 %	15.3 %
	Isen-Mom	18.5 %	24.6 %
	Mom-Mom	3.1 %	14.0 %
$\Phi_1 = \Phi_3 = 0.2$	Isen-CP	13.2 %	15.5 %
	Mom-CP	2.5 %	8.3 %
	Isen-Mom	21.5%	23.7 %
	Mom-Mom	4.9 %	8.7 %
$\Phi_1 = \Phi_3 = 0.5$	Isen-CP	11.6 %	9.7%
	Mom-CP	5.2 %	6.4 %
	Isen-Mom	25.7 %	30.6 %
	Mom-Mom	15.7 %	15.5%

Table 1: Root-mean-square percentage error for the intra-pipe restriction boundary resolution methods

As depicted in Figures 6, 7 and 8 and Table 1, the restriction model with momentum outflow and constant pressure inflow exhibits the best predictability. This result is very interesting as these two models had already shown to have a better predictability than the other models considered in this work when used separately. It is curious that the traditionally used quasi-steady model of the restriction (isentropic contraction + momentum) presents the lowest predictability. The experimental results confirm that the isentropic contraction assumption systematically over-estimates the flow speed which results in a significant disagreement with respect to the measurements. The temperature behavior of Figures 6, 7 and 8 shows that the rise of the temperature appears too early for the models with combinations using the isentropic contraction. This is because the isentropic contraction does not take into account the increase of entropy through the restriction, which allows greater flow speeds to be obtained. As the area ratio increases, the less separated the temperature curves are, as depicted in Figure 8. Two explanations are found for this behavior: first, as the area ratio increases, the faster the gas travels inside the pipe and therefore, the smaller the gap between the curves (with respect to time). A second explanation comes from the fact that as the area ratio increases, the momentum outflow model loses predictability as presented in [6].

All four simulations were carried out using the same boundary resolution method, which, as seen in the results, has effectively solved the boundary problem independently of the quasi-steady model formulation.

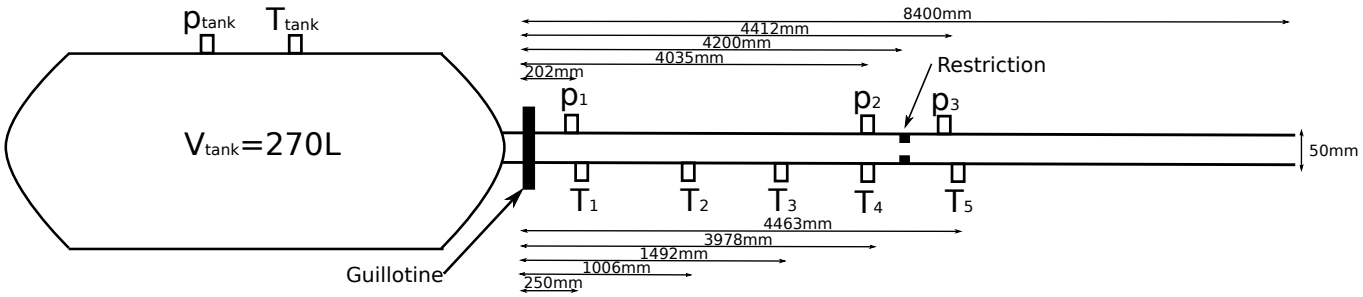

Figure 5: Schematic of the experimental setup

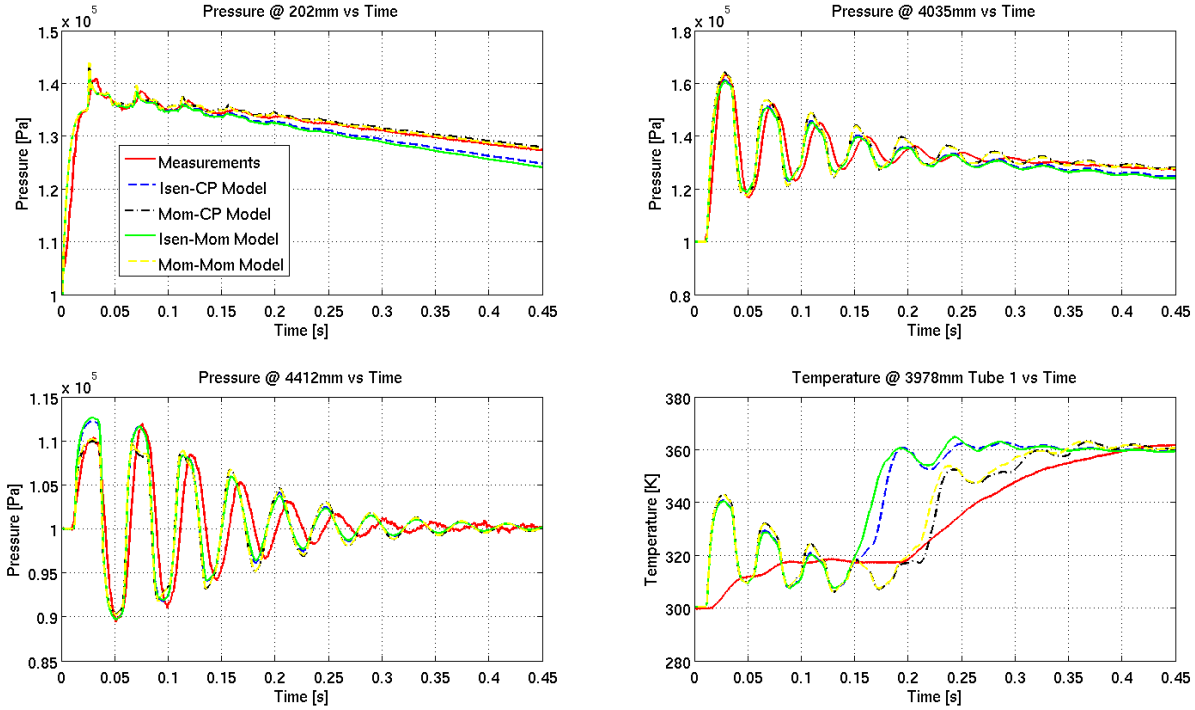

Figure 6: Validation Results for $\Phi_1 = \Phi_3 = 0.1$ and initial pressure 1.4×10^5 [Pa]

The method has successfully introduced a completely non-homentropic intra-pipe boundary resolution that performs much better (see Table 1) in terms of predictability. This illustrates the interest of using a non-homentropic formulation for the boundary resolution.

CONCLUSIONS

This paper was concerned with an intra-pipe non-homentropic boundary resolution method. A methodology for constructing restriction quasi-steady models from outflow and inflow models has been given. Building data-maps of this quasi-steady models results advantageous as no numerical method has to be introduced for solving the equation associated with the quasi-steady models. A boundary resolution method that does not take an isentropic contraction as an assumption to solve the boundary problem has been developed in order to be consistent with the non-homentropic formulation. This method is more flexible than the traditional method as different restriction quasi-steady models can be considered without changing the boundary resolution method. An experimental validation has been done with 4 different restriction quasi-steady models in order to illustrate the effectiveness of the proposed method and the gain in predictability that can be achieved without adding artificial discharge coefficients. The restriction model with momentum outflow model and constant pressure inflow model has shown to be more predictive than the order approaches considered in this work.

Due to the time response of the temperature sensors, an upgrade on the experimental setup temperature sensors is planned in order to reduce the temperature

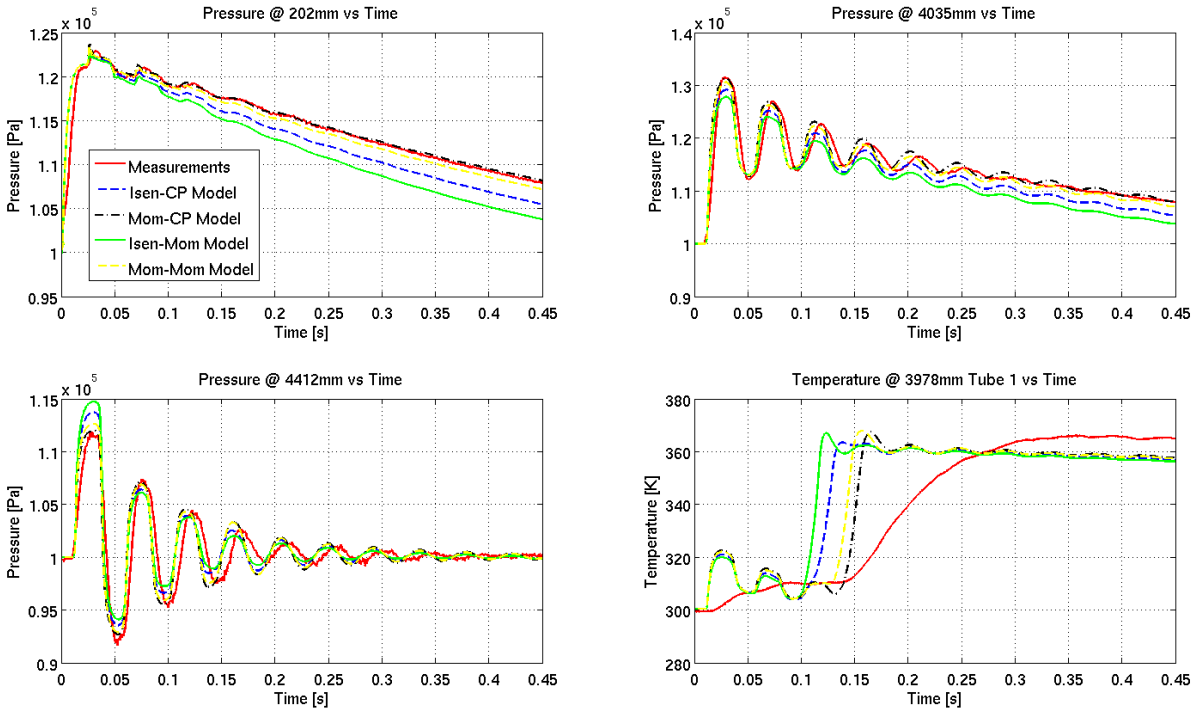

Figure 7: Validation Results for $\Phi_1 = \Phi_3 = 0.2$ and initial pressure 1.2×10^5 [Pa]

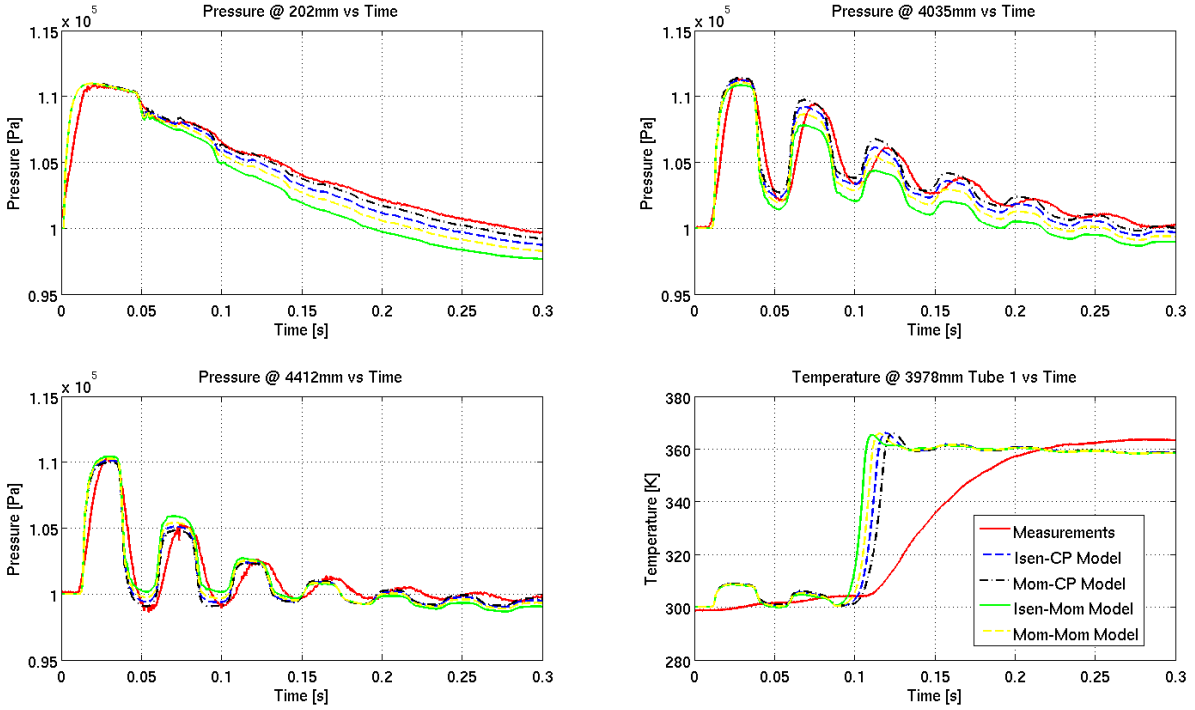

Figure 8: Validation Results for $\Phi_1 = \Phi_3 = 0.5$ and initial pressure 1.1×10^5 [Pa]

measurement time response. A numerical 3D-CFD validation could complement this work along with an experimental validation using a control valve and a variation of gas composition. The proposed boundary resolution method has been used successfully used to validate and design boundary observers and controllers

for hyperbolic systems [5]. A natural extension of this work seems to be the development of similar boundary resolution methods for other intra-pipe boundary conditions such as volumes, compressors and turbines. There are still many open questions. Creating restriction model independent boundary resolution methods capable of taking into account the dynamics at the boundaries seems to be a challenging issue.

REFERENCES

[1] K. Akihama, Y. Takatory, K. Inagaki, S. Sasaki, and A. Dean. Mechanism of the smokeless rich diesel combustion by reducing temperature. *SAE Technical Paper 2001-01-0655, doi:10.4271/2001-01-0655*, 2001.

[2] M. Alriksson and I. Denbrantt. Low temperature combustion in a heavy duty diesel engine using high levels of EGR. *SAE Technical Paper 2006-01-0075, doi:10.4271/2006-01-0075*, 2006.

[3] M. Ammann, N. Fekete, L. Guzella, and A. Glattfelder. Model-based control of the VGT and EGR in a turbocharged common-rail diesel engine: theory and passenger car implementation. *SAE World Congress, Detroit, USA, Paper 2003-01-0357*, 2003.

[4] R. Benson. *The Themodynamics and Gas Dynamics of Internal-Combustion Engines*, volume 1. Clarenton Press, 1982.

[5] F. Castillo, W. Witrant, C. Prieur, and L. Dugard. Dynamic boundary stabilization of linear and quasi-linear hyperbolic systems. *51st IEEE Control and Decision Conference*, 2012.

[6] F. Castillo, W. Witrant, V. Talon, and L. Dugard. Restriction model independent method for non-isentropic outflow valve boundary problem resolution. *SAE Technical Paper 2012-01-0676, doi:10.4271/2012-01-0676*, 2012.

[7] D. Chalet and P. Chesse. Fluid dynamic modelling of junctions in internal combustion engine inlet and exhaust systems. *Journal of Thermal Science*, 19(5):410–418, 2010.

[8] D. Chalet, P. Chesse, and J-F. Hetet. Boundary conditions modelling of one-dimensional gas dynamics flows in an internal combustion engine. *International Journal of Engine Research*, 9(4):267–282, 2008.

[9] D. Chalet, P. Chesse, and X. Tauzia J-F. Hetet. Inflow boundary condition for one-dimensional gas dynamics simulation code of internal combustion engine manifolds. *Proceedings of the Institution of Mechanical Engineers, Part D, Journal of Automobile Engineering*, 223(7):953–965, 2009.

[10] J. Chauvin, G. Corde, and N. Petit. Constrained motion planning for the airpath of a diesel HCCI engine. *Proceedings of the 45th IEEE conference on decision and control*, pages 3589–3596, 2006.

[11] G.Martin. *0-D -1-D Modeling of the air path of ICE Engines for control purposes*. PhD thesis, Universite d'Orleans, France, 2010.

[12] G.Martin, P. Brejaud, P. Higelin, and A. Charlet. Pressure ratio based method for non-isentropic inflow valve boundary condition resolution. *SAE Technical Paper 2010-01-1052, doi:10.4271/2010-01-1052*, 2010.

[13] A. Hribernik. The potential of the high and low-pressure exhaust gas recirculation. *Proceeding of the SAE conference, Paper 2002-04-0029*, 2002.

[14] I. Kolmanovski, J. Sun, and M. Druzhinina. Charge control for direct injection spark ignition engines with EGR. *Proceedings of the 45th IEEE conference on decision and control, 34-38*, 2000.

[15] T. Ryan and A. Matheaus. Fuel requirements for HCCI engine operation. *SAE transactions-Journal of Fuels Lubricants*, 112:1143–1152, 2003.

[16] Gamma Technologies. *A GT-SUITE Application for Engine Performance, Acoustics, and Control Simulation*. Gamma Technologies, 2004.

[17] J. Wang. Air fraction estimation for multiple combustion mode diesel engines with dual-loop EGR systems. *Control Engine Practice 16, 1479-1468*, 16, 2008.

[18] D.E. Winterbone and R.J. Pearson. *Theory of Engine Manifold Design: Wave Action Methods for IC Engines*. Society of Automotive Engineers. Inc, 2000.

APPENDIX I

EFFECT OF THE VARIATION OF THE HEAT RATIO ON THE INTRA-PIPE RESTRICTION MODELS

In order to illustrate the effect of the variation of the heat ratio on the intra-pipe restriction quasi-steady models, a comparison between the data-maps generated with different heat ratios is performed. As presented in Figure 2, two of the quasi-steady restriction models are used to illustrate the impact of the heat ratio variation. As this work is focused on the modeling of the EGR and admission throttles, the variation of the heat ratio is considered between 1.4 and 1.32 (heat ratios of fresh

air at $300K$ and EGR gas at $770K$ and with fresh mass fraction of 40%, respectively).

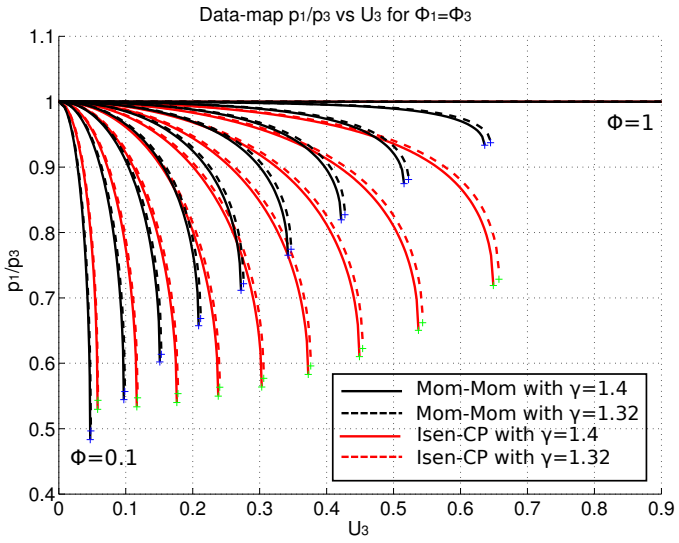

Figure 9: Intra-pipe restriction model data-map comparison for different heat ratios

As depicted in Figure 9, the effect of the variation of the heat ratio on the quasi-steady model is much smaller than the effect of the change of modeling formulation. This implies that the impact of the variation of the heat ratio on the quasi-steady models is not significant when compared with the impact of the modeling formulation (for the application considered in this work). The model variation with respect to the heat ratio is thus not considered for control and estimation purposes.

However, if the variation of the heat ratio is required, the data-map presented in (14) can be extended to take into account this variation as follows:

$$\frac{p_1}{p_3} = Datamap_p(U_3, \Phi_1, \Phi_3, \gamma) \tag{26}$$

This increases the usage of memory as well as the calculation load to solve the boundary problem, which is undesirable for control and estimation purposes.